Control of Energy Spread and Dark Current in Proton and Ion Beams Generated in High-Contrast Laser Solid Interactions

F. Dollar,[1] T. Matsuoka,[1] G. M. Petrov,[2] A. G. R. Thomas,[1] S. S. Bulanov,[1] V. Chvykov,[1] J. Davis,[2] G. Kalinchenko,[1] C. McGuffey,[1] L. Willingale,[1] V. Yanovsky,[1] A. Maksimchuk,[1] and K. Krushelnick[1]

[1]*Center for Ultrafast Optical Science, University of Michigan, Ann Arbor, Michigan 48109, USA*
[2]*Plasma Physics Division, Naval Research Laboratory, Washington, D.C. 20375, USA*

(Received 20 April 2011; published 3 August 2011)

By using temporal pulse shaping of high-contrast, short pulse laser interactions with solid density targets at intensities of 2×10^{21} W cm^{-2} at a 45° incident angle, we show that it is possible to reproducibly generate quasimonoenergetic proton and ion energy spectra. The presence of a short pulse prepulse 33 ps prior to the main pulse produced proton spectra with an energy spread between 25% and 60% ($\Delta E/E$) with energy of several MeV, with light ions becoming quasimonoenergetic for 50 nm targets. When the prepulse was removed, the energy spectra was broad. Numerical simulations suggest that expansion of the rear-side contaminant layer allowed for density conditions that prevented the protons from being screened from the sheath field, thus providing a low energy cutoff in the observed spectra normal to the target surface.

DOI: 10.1103/PhysRevLett.107.065003 PACS numbers: 52.38.Kd, 41.75.Ak, 52.50.Jm, 52.70.Nc

Laser driven ion accelerators are a promising option for applications such as ion therapy [1], fast ignition fusion [2], and proton radiography [3] due to their compact nature, small source size, and low emittance. An important mechanism for laser ion acceleration is target normal sheath acceleration (TNSA) [4,5]. In this process, an intense laser pulse incident on a solid density target will generate relativistic electrons that can propagate through the rear surface of the target setting up an electrostatic sheath with electric field strengths exceeding $\sim$1 TV m^{-1}. The nanometer thickness layer of proton-rich contaminants on the target surface first becomes ionized and subsequently is accelerated in the sheath field. Proton beams with energies of up to 17 MeV have been accelerated from short pulse interactions [6], while long pulse lasers have produced proton energies in excess of 55 MeV [5].

For most applications, a monoenergetic ion beam is desirable; however, proton and ion beams accelerated via TNSA have previously been observed with Boltzmann-like energy distributions [7,8]. Spectral modification has been observed in experiments that used complex target preparation methods [9], or energy selection [10]. Experimentally, radiation pressure driven shocks have also demonstrated narrow energy spread spectra from gas targets [11]. Recent work suggests that with only modest increases of intensity, short pulse lasers may be able to accelerate protons with narrow energy spreads to several hundreds of MeV from ultrathin ($\sim$ 10 nm) targets [12].

The use of such thin targets is limited by hydrodynamic expansion due to preheating by amplified spontaneous emission (ASE) as well as picosecond prepulses inherent in chirped pulse amplification laser systems. The ratio between the on-target intensity of these pedestals and that of the primary pulse is known as the laser ''contrast.'' A lower limit to the target thickness exists which is due primarily to the influence of the laser contrast [13] as strong prepulses from poor laser contrast can cause drastic and uncontrollable changes to the density profile.

In this Letter we demonstrate a technique for controlling the ion energy spectra that requires no prior manipulation of the target, nor the need for exotic targets. A pulse with $\leq 10^{-13}$ ASE intensity contrast interacts with silicon nitride (Si_3N_4) membranes from 30–200 nm or with Mylar ($C_{10}H_8O_4$) from 1 to 13 μm to produce exponential proton energy spectra to energies up to 9.5 MeV. We demonstrate that if the high intensity interaction is preceded by a much less intense short pulse prepulse 33 ps prior to the main pulse, the proton energy spectra becomes narrowed. This is due to keV electrons generated from this prepulse that are able to collisionally ionize the rear-side contaminant layer, causing expansion and a reduction in density. From this picosecond scale window, only the ions with a high charge-to-mass ratio ($\frac{q}{m}$) are able to move significantly, so that the lightest ions in the contaminant layer preferentially expand while the target remains mostly unperturbed, in contrast to the hydrodynamic expansion that occurs from ASE prepulse interactions. Changing the percentage of protons in the contaminant layer [14], as well as multiple intense short pulses [15], has previously been shown in simulations to cause a quasimonoenergetic spectrum in protons.

The experiments were performed using the HERCULES facility at University of Michigan, a Ti:sapphire laser system ($\lambda = 800$ nm) that produces pulses with $\tau =$ 30 fs duration FWHM with an ASE intensity contrast of 10^{-11} [16]. For additional contrast improvement we employ ''plasma mirrors,'' in which a laser pulse is focused onto a low reflectivity, optically flat substrate positioned so

that light arriving before the main pulse is transmitted while the main pulse reaches sufficient intensity to form a plasma that maintains the optical quality of the substrate for the duration of the short pulse [17]. Plasma mirror characterizations for short pulses have demonstrated up to 70% reflectivity while maintaining the wave front and decreasing the contrast by $\sim 10^2$ [18]. In our experiment, two antireflecting BK7 glass substrates are used which act as plasma mirrors. Each plasma mirror reflects less than 0.5% at 810 nm while possessing a measured reflectivity of between 65% and 70% after the formation of a plasma on the mirror surface. High speed diode measurements (temporal resolution of 1 ns) allow for the measurement of the energy contrast between the ASE pedestal and the main pulse, which can then infer an ASE intensity contrast of less than 10^{-13} on target, well below the damage threshold of the targets used. The picosecond contrast profile is measured with a third order autocorrelator before the plasma mirrors [16]. The laser energy was 1.1 ± 0.1 J on the target with approximately 65% of the energy in a 1.2 μm focal spot FWHM via an $f/1$ off-axis parabolic mirror. This corresponds to an on-target intensity of 2×10^{21} W cm^{-2} with a normalized vector potential of $a_0 = 30$. The near diffraction limited focus with Strehl ratio between 0.6 to 0.9 was measured with a Shack-Hartmann sensor and was wave front corrected by using a deformable mirror (Xinetics).

Deliberate introduction of a short prepulse can be achieved simply by introducing a postpulse prior amplification. Nonlinear interactions between the postpulse and the main pulse during amplification resulted in a prepulse after compression [19]. This nonlinearly generated prepulse will henceforth be simply referred to as the prepulse. The prepulse arrived 33 ps prior to the main pulse as measured by a streak camera. The on-target peak intensity of this prepulse is measured to be $3(\pm 2) \times 10^{16}$ W cm^{-2} with a 30 fs duration. Images of the laser beam profile after the plasma mirror indicate that this prepulse generates some plasma on the surface of the first plasma mirror, but the resulting focal spot is not measurably degraded. While other short pulse prepulses exist [16], the intensity after the plasma mirrors is below the damage threshold of the targets used. The targets used were freestanding Si_3N_4 membranes and Mylar foils, which have a similar damage threshold. The targets were positioned at the laser focus with an accuracy of ± 2 μm at an angle of incidence of 45°. The beam was p polarized. Beam profile diagnostics were used to determine energy throughput and ASE contrast enhancement. A Thomson parabola ion spectrometer (TP) was the primary diagnostic for the measurements of ion energy spectra [20]. Parallel electric and magnetic fields disperse the ion traces, the separation of which is dependent on the $\frac{q}{m}$ of the ion species. The solid angle subtended by the TP is 9.6×10^{-8} sr in the target normal direction. Error increases with increasing energy, as the dispersion decreases with higher ion energy. A microchannel plate was used as the detector.

Proton and carbon spectra are characterized in this experiment, although oxygen and nitrogen were observed to be present as well. The traces, such as those shown in Figs. 1(c) and 1(d), are displaced in one axis by the $\frac{q}{m}$, and in another by the charge-to-momentum ratio, measured relative to a zero order spot produced by neutral particles and photons. Characteristic in measurements of clean pulse spectra was a peak in an otherwise Boltzmann-like energy spectrum [Fig. 1(b)]. As the target thickness is decreased, the maximum observed proton energy increased from 6.7 (± 1.3) MeV at 1 μm thickness to 9.5 (± 3.3) MeV at 30 nm target thickness (Fig. 2). We observed a trend such that thinner targets produce higher energies, as the electron density in the sheath increases and can provide stronger accelerating fields, consistent with previous results [13]. The other ions display a similar trend in their maximum energy.

For the prepulse case, the proton energy spectra show significant qualitative differences, namely, that the low energy protons are below the detection threshold of the TP [Fig. 1(d)]. For the 50 nm Si_3N_4 targets, ions also exhibit the narrow energy spread feature. The FWHM of the proton spectral peak varies minimally, although the maximum energy of the spectra is dependent on target thickness [Fig. 2(b)]. It is also observed that the energy spread ($\frac{\Delta E}{E}$) varies from shot to shot between 25% and 60%. At target thickness of 1 μm both prepulse and clean pulse produce similar energy protons, but for the submicron targets peak proton energies fail to increase in the prepulse case [Fig. 2(c)], indicating that the prepulse is likely causing significant deformation of the bulk target before the arrival of the main pulse. When the target is defocused or at normal incidence, a broad energy spectrum returns, suggesting that this phenomena is dependent on

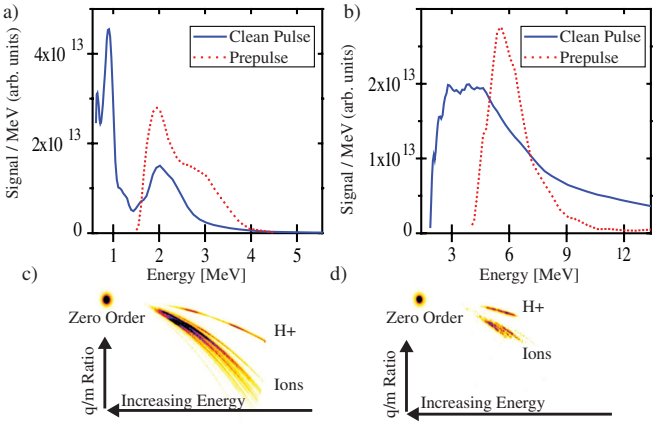

FIG. 1 (color online). Energy spectra for prepulse (50 nm Si_3N_4) and clean pulse (30 nm Si_3N_4) for (a) protons and (b) carbon 4 + . The sharp drop on the clean pulse case is due to the edge of the detector. The raw traces for these spectra are also shown for (c) clean pulse and (d) prepulse.

intensity and the target being at an oblique angle [Fig. 2(a)]. Laser transmission remained below background for all target thicknesses, indicating that targets were above critical density, or n_{crit}, the density above which the plasma can no longer support propagating light waves, until main pulse interaction. CR-39 track detectors were used to measure the divergence of the proton beams produced. In both cases the divergence was measured to be below 250 mrad for 1 MeV and below 75 mrad for 5 MeV protons.

The quasimonoenergetic feature in the proton energy spectra is highly reproducible, for example, being observed in 71 out of 95 shots taken over several shot days for all target thicknesses when the prepulse is present [Fig. 2(b)]. Since the effect is observed to be the same in both the nonhydrogen containing Si_3N_4 targets as well as Mylar, the accelerated ions are thought to be generated entirely from contaminants on the surface of the target rather than from the bulk target itself. The effect is only observed for oblique angles, as expected due to the angular dependence of laser absorption processes.

Numerical modeling is difficult due to the 33 ps time scale between pulses, the high density, and the fact that a hydrodynamic simulation will not correctly model hot electron transport. For a prepulse with intensity of $>10^{16}$ W cm^{-2}, a combination of inverse bremsstrahlung and Brunel heating [21] will create a localized plasma and a population of hot electrons with a mean kinetic energy of $T_h = 3.6 I_{16} \lambda_\mu^2 \approx 6$ keV [22], which we have also validated with particle-in-cell (PIC) simulations using the OSIRIS code [23]. To estimate the field strength on the rear of the target for the 13 μm thick Mylar case, we used an implicit 2D Vlasov-Fokker-Planck code [24,25] modified to include a collisional Saha ionization model and a nonrelativistic Bethe collisional energy loss formula for the un-ionized material to numerically model the electron transport and ionization dynamics in the target. The anticipated electric field is expected to be too weak for field ionization to have a significant impact, so it was not included in the code. Ionization of the target at this intensity may also be affected by radiative energy transfer [26]. Suprathermal electrons from the tail of the front surface plasma propagate through the target and set up a sheath electric field of strength $\sim 10^8$ V m^{-1} on the rear surface, indeed several orders too low to cause field ionization.

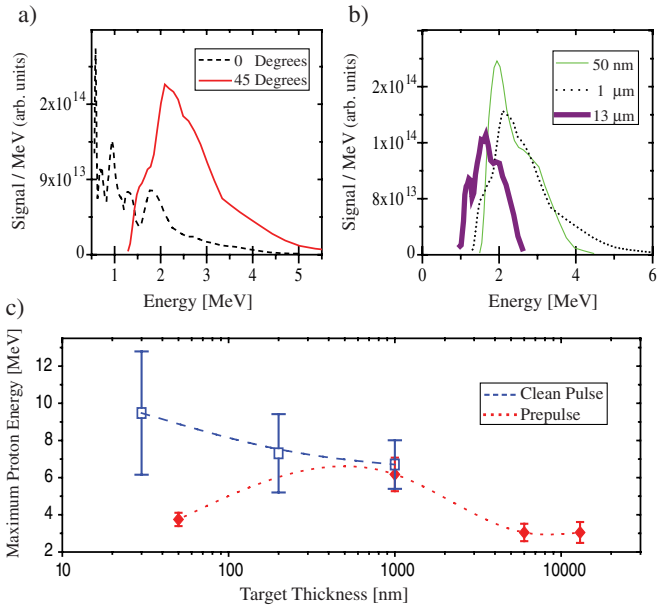

FIG. 2 (color online). (a) Proton spectra for prepulse case for 0° and 45° incidence for 1 μm Mylar targets. (b) Prepulse proton spectra for 3 target thicknesses. (c) Maximum proton energy for prepulse and clean pulse case. Lines are shown for visual aid only.

Although the electron distribution function at the rear is a two temperature distribution, rather than a single temperature commonly used in self-similar expansion models, we can use an average over the hot and cold populations to calculate the sound speed [27]. Then in a single temperature expansion model, we can estimate the plasma scale length λ_s at 33 ps via $\lambda_s \approx 2 c_s t$ [7], where $c_s^2 = Z k_B \langle T_e \rangle / m_i$ and $\langle T_e \rangle = (n_{eh} T_{eh} + n_{ec} T_{ec})/n_e$ with the subscripts referring to hot and cold electrons. This gives an exponential profile with a scale length of the order 100 nm using the temperature and density outputs from the 2D Vlasov-Fokker-Planck simulation, although we expect this to be an upper limit. Protons will have a much longer scale length than the other ions due to their much higher $\frac{q}{m}$.

For PIC simulations of the main pulse interaction, a 1.2 μm fully ionized carbon target with density of $100 n_{\mathrm{crit}}$ was used with front- and rear-side proton layers. For simplicity, the scale lengths are linear ramps, with the density referring to the maximum density of the ramp with total integrated density constant and the thickness as the base of the ramp from the bulk target. A 45° p-polarized Gaussian laser pulse with 35 fs FWHM duration, 1.2 μm waist, and a field strength parameter of $a_0 = 30$ was focused onto a target with a front-side proton scale length of 300 nm. The cell size was 2.55 nm × 3.8 nm, or $\lambda/315$. 128 particles per cell were used for the proton layer, with 16 particles used in all other cells.

The scale length of rear surface plasma for the prepulse case is 175 nm and has a proton density of $0.3 n_{\mathrm{crit}}$, while for the clean pulse the scale length is 2 nm and the maximum density is $60 n_{\mathrm{crit}}$. In the first case, the low rear-side proton density results in minimal electric field screening due to the longer Debye length. The field is quasistatic, and protons closest to the target will be in the accelerating field longer, thus having higher energies. This is evident in the phase space plots of the rear protons, which show a narrow momentum spread [Fig. 3(c)], and also in the proton density, where protons closest to the target eventually overlap the ion front. The protons possessing zero tangential velocity and thus those moving in

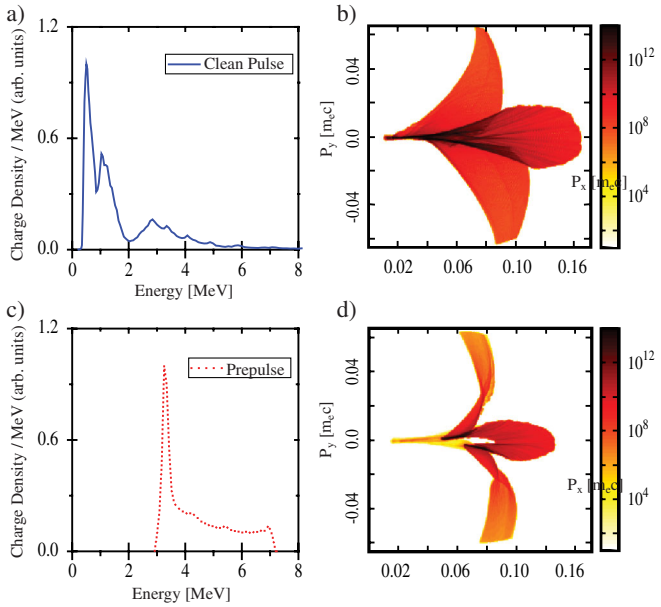

FIG. 3 (color online). PIC simulation results at 202 fs of proton energy spectra for clean pulse (a) and prepulse (c) for 1 μm carbon target at target normal ($p_y \approx 0$) with charge density individually normalized to 1 for comparison. Proton phase space P_x vs P_y are also shown for clean pulse (b) and prepulse (d) in units of normalized momentum. Note that the color scale is logarithmic.

target normal have a quasimonoenergetic spectrum, with energies ranging from 3–7.2 MeV. In the simulation, at angles other than directly at target normal the spectrum shows increased energy spread.

In the clean pulse PIC simulation, the rear-side protons initially move as a layer but spread out as they travel. In this case, the sheath field is time varying due to proton screening, in contrast to the prepulse case. Since the contaminant layer is thicker than the cold Debye length (≈ 1 nm), protons in the layer can experience different forces. In this case the protons closest to the target experience the least acceleration and provide the low energy component of the spectrum. The spectrum also displays a peaked structure similar to what is observed experimentally [Fig. 3(a)] and also shows higher maximum energy than the prepulse case. As the simulated target is 1.2 μm in thickness, this peak is likely an artifact of a thin proton layer undergoing rapid acceleration, making it an experimental cue for short pulse experiments that high contrast has been achieved. For very thin targets, it is likely that the expansion can be sufficient for the light ions to be of low enough density to also display quasimonoenergetic features, as observed in experiment.

In conclusion, we have demonstrated control of the spectral shape of the proton and ion beams via the introduction of a high-contrast short pulse prepulse 33 ps prior to a high intensity laser interaction and without prior target manipulation. As opposed to poor contrast experiments, the prepulse is able to shape the density of the contaminant layer without significantly affecting the bulk target. Proton beams with maximum energy of up to 6.2 MeV were produced with as low as 30% energy spread and a suppressed dark current of low energy ions. Simulations were performed at high resolution for conditions matching the experiment, reproducing the spectral shaping that is observed experimentally and providing insight into the acceleration mechanisms that produced the observed narrow spectral features. The experiment was performed with a fixed prepulse delay, which limited the target thickness, but this delay could potentially be optimized for different applications.

This work was supported by the NSF through the Physics Frontier Center FOCUS (Grant No. PHY-0114336), as well as by the Defense Threat Reduction Agency and the Naval Research Laboratory. We acknowledge the OSIRIS consortium (UCLA/IST Portugal) for the use of OSIRIS. Simulations were performed on the Nyx Cluster at the University of Michigan.

[1] S. V. Bulanov *et al.*, Phys. Lett. A **299**, 240 (2002); E. Fourkal *et al.*, Med. Phys. **29**, 2788 (2002); V. Malka *et al.*, *ibid.* **31**, 1587 (2004).
[2] M. Roth *et al.*, Phys. Rev. Lett. **86**, 436 (2001); V. Yu. Bychenkov *et al.*, Plasma Phys. Rep. **27**, 1017 (2001); J. Davis *et al.*, Plasma Phys. Controlled Fusion **53**, 045013 (2011).
[3] M. Borghesi *et al.*, Rev. Sci. Instrum. **74**, 1688 (2003).
[4] E. L. Clark *et al.*, Phys. Rev. Lett. **84**, 670 (2000); A. Maksimchuk *et al.*, *ibid.* **84**, 4108 (2000); S. C. Wilks *et al.*, Phys. Plasmas **8**, 542 (2001).
[5] R. A. Snavely *et al.*, Phys. Rev. Lett. **85**, 2945 (2000); S. P. Hatchett *et al.*, Phys. Plasmas **7**, 2076 (2000).
[6] K. Zeil *et al.*, New J. Phys. **12**, 045015 (2010).
[7] P. Mora, Phys. Rev. Lett. **90**, 185002 (2003).
[8] M. Allen *et al.*, Phys. Rev. Lett. **93**, 265004 (2004).
[9] B. M. Hegelich *et al.*, Nature (London) **439**, 441 (2006); H. Schwoerer *et al.*, Nature (London) **439**, 445 (2006).
[10] T. Toncian *et al.*, Science **312**, 410 (2006).
[11] C. Palmer *et al.*, Phys. Rev. Lett. **106**, 014801 (2011); D. J. Haberberger *et al.*, in Proceedings of the 2011 Particle Accelerator Conference, New York, http://www.c-ad.bnl.gov/pac2011/proceedings/papers/tuobn6.pdf, paper TUOBN6.
[12] T. Esirkepov *et al.*, Phys. Rev. Lett. **92**, 175003 (2004); A. P. L. Robinson *et al.*, New J. Phys. **10**, 013021 (2008); A. Macchi, S. Veghini, and F. Pegoraro, Phys. Rev. Lett. **103**, 085003 (2009); S. S. Bulanov *et al.*, Phys. Rev. E **78**, 026412 (2008); A. Henig *et al.*, Phys. Rev. Lett. **103**, 245003 (2009).
[13] M. C. Kaluza *et al.*, Phys. Rev. Lett. **93**, 045003 (2004).
[14] A. P. L. Robinson, A. R. Bell, and R. J. Kingham, Phys. Rev. Lett. **96**, 035005 (2006).
[15] A. P. L. Robinson *et al.*, Plasma Phys. Controlled Fusion **49**, 373 (2007).
[16] V. Chvykov *et al.*, Opt. Lett. **31**, 1456 (2006).

[17] B. Dromey *et al.*, Rev. Sci. Instrum. **75**, 645 (2004).
[18] R. Hörlein *et al.*, New J. Phys. **10**, 083002 (2008); G. Doumy *et al.*, Phys. Rev. E **69**, 026402 (2004).
[19] X. Liu *et al.*, Opt. Lett. **20**, 10 (1995).
[20] J. J. Thomson, Philos. Mag. **21**, 225 (1911).
[21] F. Brunel, Phys. Rev. Lett. **59**, 52 (1987).
[22] P. Gibbon *et al.*, Plasma Phys. Controlled Fusion **38**, 769 (1996).
[23] R. O. Fonseca *et al.*, Lect. Notes Comput. Sci. **2331**, 342 (2002).
[24] A. G. R. Thomas *et al.*, New J. Phys. **11**, 033001 (2009).
[25] R. J. Kingham *et al.*, J. Comput. Phys. **194**, 1 (2004).
[26] T. Ditmire *et al.*, Phys. Rev. Lett. **77**, 498 (1996).
[27] M. Passoni *et al.*, Phys. Rev. E **69**, 026411 (2004).